







# Mapping blood traits to structural organization of the brain in rhesus monkeys

Yue Cui <sup>1,2,3</sup>, Haibin Huang <sup>1,2,3</sup>, Jinquan Gao <sup>4,5</sup>, Tianzi Jiang <sup>1,2,3,6</sup>, Chen Zhang <sup>7,\*</sup>, Shan Yu <sup>1,2,3,\*</sup>

<sup>1</sup>Brainnetome Center and National Laboratory of Pattern Recognition, Institute of Automation, Chinese Academy of Sciences, Beijing 100190, China,

<sup>2</sup>CAS Center for Excellence in Brain Science and Intelligence Technology, Institute of Automation, Chinese Academy of Sciences, Beijing 100190, China,

<sup>3</sup>School of Artificial Intelligence, University of Chinese Academy of Sciences, Beijing 100049, China,

<sup>4</sup>Model R&D Center, Life Biosciences Company Limited, Beijing 100176, China,

<sup>5</sup>Technology Management Center, SAFE Pharmaceutical Technology Company Limited, Beijing 100176, China,

<sup>6</sup>Key Laboratory for Neuroinformation of Ministry of Education, School of Life Science and Technology, University of Electronic Science and Technology of China, Chengdu 610054, China,

<sup>7</sup>Department of Neurobiology, School of Basic Medical Sciences, Beijing Key Laboratory of Neural Regeneration and Repair, Advanced Innovation Center for Human Brain Protection, Capital Medical University, Beijing 100069, China

\*Corresponding author: Shan Yu, Institute of Automation, Chinese Academy of Sciences, 95 Zhongguancun East Rd, Haidian District, Beijing 100190, China. Email: shan.yu@nlpr.ia.ac.cn; Chen Zhang, Room 626, School of Basic Medical Sciences, Capital Medical University, Beijing 100069, China. Email: czhang@ccmu.edu.cn

Hematological and biochemical blood traits have been linked to brain structural characteristics in humans. However, the relationship between these two domains has not been systematically explored in nonhuman primates, which are crucial animal models for understanding the mechanisms of brain function and developing therapeutics for various disorders. Here we investigated the associations between hematological/biochemical parameters and the brain's gray matter volume and white matter integrity derived from T1-weighted and diffusion magnetic resonance imaging in 36 healthy macaques. We found that intersubject variations in basophil count and hemoglobin levels correlated with gray matter volumes in the anterior cingulum, prefrontal cortex, and putamen. Through interactions between these key elements, the blood parameters' covariation network was linked with that of the brain structures, forming overarching networks connecting blood traits with structural brain features. These networks exhibited hierarchical small-world architecture, indicating highly effective interactions between their constituent elements. In addition, different subnetworks of the brain areas or fiber tracts tended to correlate with unique groups of blood indices, revealing previously unknown brain structural organization. These results provide a quantitative characterization of the interactions between blood parameters and brain structures in macaques and may increase the understanding of the body–brain relationship and the pathogenesis of relevant disorders.

**Key words:** gray matter; hematology; rhesus monkey; serum biochemistry; white matter.

## Introduction

Hematological and biochemical parameters are useful markers of physical health conditions in both humans and animals. Hematological parameters, including leukocyte, erythrocyte, and platelet measures, are usually considered to be useful indicators of immune responses (Curran et al. 2017). Biochemical indices consist of a number of biochemical components and enzyme activities and can reflect biochemical processes, biomolecule transport, and enzyme functions (Burtis et al. 2012). Studies have shown that blood traits, including hematological and biochemical parameters, are linked to the occurrence of various brain disorders such as stroke (Harshfield et al. 2020), Alzheimer's disease (Mapstone et al. 2014; Nägga et al. 2018; Gokce et al. 2019), and other neurovascular and neurodegenerative disorders (Kalay et al. 2012; Nambron et al. 2016). Importantly, in the absence of disease or high risk, some blood variations have also been shown to be associated

with brain structures in humans (Williams et al. 2013; Schilling et al. 2014), suggesting profound interactions between the body and the brain. Specifically, blood variations have been reported as being associated with gray matter (GM) volume (Qiu et al. 2012), white matter (WM) integrity (Williams et al. 2013; Power et al. 2017), and WM hyperintensity (Schilling et al. 2014). However, the previous results in humans were inconsistent. For instance, elevated serum cholesterol levels were reported to be related to a decrease in total gray matter volume (Whalley et al. 2003). This association was found in the medial temporal regions but only in male subjects (Qiu et al. 2012). In contrast, some studies suggested positive correlations between cholesterol and the medial temporal regions. For instance, medial temporal gray matter volumes were positively correlated with cholesterol levels in a group of healthy individuals with low cholesterol levels (< 200 mg/dl) (Yang et al. 2020). Other studies found positive correlations between

cholesterol and cortical thickness across the brain (Leritz et al. 2011) or in the fronto-parietal and occipital areas (Coutinho et al. 2017) in healthy middle-aged to older adults, suggesting positive effects of cholesterol on brain function. This inconsistency may possibly be related to the impact of sample heterogeneity, such as differences in socio-demographics, diet, lifestyle, and environmental factors.

Although some information has become available through human studies, systematic analyses of the relationship between hematological and biochemical parameters and brain structures in nonhuman primates (NHPs) are still quite limited. NHPs are important models for understanding the mechanisms of higher brain function and pathology of related disorders. Experimental NHPs are generally housed in stable environments with standardized diets, providing unique conditions for studying the intrinsic link between systemic factors, e.g. hematological and biochemical parameters and brain structure and function. The rhesus monkey (*Macaca mulatta*) is a commonly used NHP because its genetics, physiology, neural architecture, and behaviors are strikingly similar to those of humans (Gibbs et al. 2007). Macaques have the major advantage of having brains with comparable neuroanatomical and connectivity to those of humans (Van Essen et al. 2019) and possess sensorimotor and cognitive functions that more closely resemble those of humans (Gray and Barnes 2019). Therefore, they are preferred animal models for unraveling the intrinsic link between blood factors and the brain.

NHP neuroimaging is a noninvasive technique that can characterize brain organization and function and can be used in comparative and translational neuroscience (Rilling 2014; Vanduffel et al. 2014; Xu et al. 2018; Xu et al. 2020). Subtle morphometric changes can be captured by T1-weighted images, which have been used to examine total and regional volumetric changes during both development (Scott et al. 2016) and aging (Alexander et al. 2008; Chen et al. 2013). Diffusion magnetic resonance imaging (dMRI) quantifies microstructural information about white matter integrity and coherence by assessing fractional anisotropy (FA), which represents the degree of directed water diffusion and may reflect myelination (Sampaio-Baptista et al. 2013) and fiber geometry (Tuch et al. 2005). Evidence has shown increased FA with age during development (Kim et al. 2020) and reduced FA in aging rhesus monkeys (Makris et al. 2007). Although previous studies have reported a relationship between a few blood indices and MRI features in macaques (Willette et al. 2012), comprehensive analyses of the relationship between these 2 domains are largely missing, and these are much needed to facilitate using NHPs as disease models in translational neuroscience.

To address this issue in the present study, we leveraged T1-weighted and dMRI imaging of macaques to investigate associations between blood parameters and gray matter volumes and white matter integrity, respectively.

Graph-theoretical analyses were applied to uncover the relationship between the covariation networks of these 2 domains. We further described novel structural organizations that depended on the similarity of diverse associations between the hematologic/biochemical parameters and the gray/white matter properties. This study may provide baseline reference indices for macaque models focusing on the central nervous system, give insights into the interactions between blood traits and the brain, and enable neurobiological comparisons between species.

## Materials and methods

### Animals

The study included a total of 36 healthy macaques (*M. mulatta*) (all males; age: 4–15 years old; weight: 4.1–11.7 kg). The monkeys were housed individually in stainless steel cages in animal rooms in an 18–26 °C environment and 40–70% relative humidity. Fresh air and daily light–dark cycles were maintained in the animal rooms. The animals were fed formula food for experimental monkeys and fresh fruits and had freely available drinking water. All the animals were negative for *Mycobacterium tuberculosis*, *Salmonella Typhi*, *Shigella dysenteriae*, pathogenic dermatophytes, and herpes B virus. The monkeys were divided into three age groups in the present study: young adults, 4–6 years old ( $n = 12$ ); adults, 8–9 years old ( $n = 12$ ); and middle-aged adults, 14–15 years old ( $n = 12$ ). This study was approved by the Institutional Review Board/Ethics Committee of Capital Medical University (No. AEEI-2019-077).

### Blood sample collection and preparation

After overnight fasting (around 14 h), awake monkeys were restrained by experienced animal care technicians, and 5 mL blood samples were collected from the upper forearm. About 2 mL were transferred into ethylenediaminetetraacetic acid-potassium (EDTA-K2) tubes for hematological analysis. The remaining 3 mL aliquots were stored in plastic tubes without anticoagulants for biochemical analysis. The latter aliquots were allowed to clot at room temperature for 30 min, and the serum was separated by centrifugation at 1600 g for 15 min and analyzed immediately. Blood collections were performed twice at an interval of 17–20 days.

### Hematological and biochemical analyses

The hematological analysis was performed using a DxH 800 automated hematology analyzer (Beckman Coulter, Miami, FL). A total of 20 parameters were included in the hematological analysis: basophil count (BASO#), basophilic leukocyte percentage (BASO%), eosinophil count (EO#), eosinophil percentage (EO%), hematocrit (HCT), hemoglobin (HGB), lymphocyte count (LYMPH#), lymphocyte percentage (LYMPH%), mean corpuscular hemoglobin (MCH), mean corpuscular hemoglobin concentration (MCHC), mean corpuscular volume (MCV), mean platelet volume (MPV), monocyte

count (MONO#), monocyte percentage (MONO%), neutrophil count (NEUT#), neutrophil percentage (NEUT%), platelets (PLT), red blood cell number (RBC), red blood cell volume distribution width (RDW), and white blood cell number (WBC).

Serum biochemical analysis was conducted using an AU5831 chemistry analyzer (Beckman Coulter, Miami, FL). Biochemical parameters included 32 parameters, including alanine aminotransferase (ALT), albumin (ALB), albumin/globulin (A/G), alkaline phosphatase (ALP), aspartate aminotransferase (AST), AST/ALT, apolipoprotein A1 (ApoA-1), apolipoprotein B (ApoB), blood urea nitrogen (BUN), creatine kinase (CK), creatine kinase myocardial band (CK-MB), creatinine (CREA), direct bilirubin (DBIL), free fatty acids (FFA), gamma glutamyl transferase (GGT), globulin (GLB), glucose (GLU), high-density lipoprotein-cholesterol (HDL-C), homocysteine (HCY), hypersensitive C-reactive protein (hs-CRP), indirect bilirubin (IDBIL), lactate dehydrogenase (LDH), lipoprotein a (LpA), low-density lipoprotein-cholesterol (LDL-C), phospholipids (PLIP), total bile acid (TBA), total bilirubin (TBIL), total cholesterol (TC), total protein (TP), triglycerides (TG), uric acid (UA), and small dense low-density lipoprotein-cholesterol (sdLDL-C).

### MRI data acquisition

The in vivo MRI scans for macaques were acquired from a Siemens Prisma 3 T MR scanner (Erlangen, Germany). Each animal underwent MRI imaging before the first blood collection. The monkeys were anesthetized with an intramuscular injection of Zoletil 50 (10 mg/kg) before scanning and were maintained under anesthesia using 0.5% isoflurane in oxygen during image acquisition. The animals were placed in a sphinx position during the scan, with an MRI-compatible stereotaxic frame optimized for the NHP head. A custom manufactured coil (Shanghai Chenguang Medical Technology) for primates was used. T1-weighted scans were obtained with a magnetization-prepared rapid gradient-echo (MPRAGE) pulse sequence using the following optimized parameters: repetition time (TR)/echo time (TE) = 2200/3.68 ms, flip angle = 8°, matrix size = 256 × 256, and slice thickness = 0.5 mm with no inter-slice gap, yielding 0.5 × 0.5 × 0.5 isotropic voxels. The acquisition parameters for the dMRI data included: TR/TE = 3,780/66 ms, flip angle = 180°, matrix size = 82 × 90, voxel size = 1.3 × 1.3 × 1.43 mm<sup>3</sup>. For each subject, a total of 65 volume were acquired, including 1 nondiffusion-weighted volume ( $b = 0$  s/mm<sup>2</sup>) and 64 noncollinear gradient directions ( $b = 1,000$  s/mm<sup>2</sup>).

### MRI data analyses

The T1-weighted MR data were preprocessed using Advanced Normalization Tools (ANTS, <http://stnava.github.io/ANTS>) to automatically remove the noise (DenoiseImage) and then correct intensity inhomogeneity artifacts (N4BiasFieldCorrection). To ensure accurate brain masks and anatomical registration for macaques, the T1-weighted images were first processed

with AFNI @animal\_warper pipeline (Jung et al. 2021) and then manually edited using ITK-SNAP (<http://www.itksnap.org/pmwiki/pmwiki.php>). Different tissue maps, including GM, WM, and cerebrospinal fluid (CSF) images in native space, were segmented using Statistical Parametric Mapping (SPM12, Wellcome Department of Imaging Neuroscience, London, UK; <http://www.fil.ion.ucl.ac.uk/spm/>). Since the tissue probability maps (TPMs) implemented in SPM12 were for humans, we used the macaque TPMs provided by Rohlfing et al. (2012). The TPMs represent the probabilities of finding GM, WM, and CSF at each voxel and are suitable for tissue segmentation because the age range of the animals used for their TPM constructions is similar to those of the samples used in our study. In addition, we calculated the contrast to noise ratio and GM/WM data homogeneity and found no group differences in the contrast to noise ratio or the GM/WM data homogeneity based on age (Supplementary Fig. S1).

The dMRI data were preprocessed using MRtrix3 (Tournier et al. 2012). First, the noise and Gibb's ringing artifacts were removed. The images were then corrected for motion and eddy current distortions. Diffusion tensors were fitted to the dMRI data, enabling the computation of an FA image for each subject. To ensure accurate anatomical registration, the skull-stripped T1-weighted image was aligned with the b0 volume and diffusion images. The diffusion-weighted data for each subject were visually inspected to ensure there were no apparent artifacts arising from the acquisition or processing procedures.

We also extracted the regions of interest (ROIs) in the GM and FA images based on the macaque brain atlas (Feng et al. 2017) and included parcellations of the cerebral cortex, subcortical regions, and white matter tracts. The ROIs in the left and right hemispheres were combined. These resulted in a total of 43 GM and 38 WM regions across the whole brain (Supplementary Fig. S2 and Table S1). We used the ANTS registration tool to transform the atlas in standard space to each subject's anatomical image, providing a parcellation of each macaque brain in native space. The sum of the GM volumetric values and the average of the FA in each ROI were calculated for each subject.

### Correlation analyses

Statistical analyses were conducted with Python 3.9 using the Pingouin package (v.0.3.11, <https://pingouin-stats.org/index.html>). Values that were 3 SD above or below the means were outliers and were removed. The demographic, hematological, and biochemical characteristics of the young adult, adult, and middle-aged adult macaques were compared using analysis of variance.

The values of hematological/biochemical parameters, GM volume, and WM integrity were z-scored for correlation analyses. Partial Pearson's correlations were used to assess the relationships between each

hematological/biochemical variable and age (adjusted for body weight and total intracranial volume (TIV)), TIV (adjusted for age and body weight), and total and ROI-based gray and white matter features (adjusted for age and TIV), separately. To determine the reliability between the two repeated measurements for each blood parameter, paired *t* tests were performed across the animals by age group to detect changes in mean values. The parameters showing no variations in the first and second measurements were retained and the average of the two measurements for these stable parameters were used in the correlation analyses. To test whether the blood parameters showed a greater correlation with age or neuroimaging features than expected by chance, 10,000 permutations were performed for each of them. A permutation test is a type of nonparametric statistical significance test that does not require making any assumptions about the sample distribution. Specifically, we first computed the partial Pearson's correlation (real correlation coefficient) for variables *X* and *Y*. Variable *X* was then permuted for 10,000 times, and we calculated the partial Pearson's correlations for each permuted *X* and *Y*. The two-sided *P* value was calculated by counting the proportion of the permuted data whose correlation coefficient was at least as great as the real correlation coefficient. To correct for multiple comparisons, a false discovery rate (FDR) approach with a threshold of  $P < 0.05$  was used to identify significant correlations between biochemical/hematological parameters and the structural features of the brain.

We also conducted graph-theoretical analyses of several covariation networks to explore the overview associations between the blood traits and brain structures. Specifically, the blood module was constructed by pairwise correlations between blood parameters and then thresholded by  $P < 0.01$  to produce a binary subnetwork. The brain module was constructed using pairwise correlations between gray/white matter ROIs and then thresholded by  $P < 0.01$  to generate a binary subnetwork. Significant correlations ( $P < 0.05$ ) between blood parameters and brain structures were deemed to be connections between the two modules. Degree centrality, defined as the fraction of nodes to which it is connected, was used to identify the hubs for each module. The edge density (ED) and small-world property were calculated for each graph. ED was defined as the number of actual connections divided by the total number of possible connections. To measure small-worldness, we calculated the coefficients  $\sigma$  as follows:

$$\sigma = \frac{C/C_{\text{rand}}}{L/L_{\text{rand}}}, \quad (1)$$

where *C* and *L* are the average clustering coefficient and average shortest path length of the original network, respectively.  $C_{\text{rand}}$  and  $L_{\text{rand}}$  are the corresponding values for an equivalent random network. A network has small-world property if  $\sigma > 1$ .

## Blood clustering by covariation with GM and WM

Similarity matrices between the covariation patterns of all the blood parameters with the ROI-based GM/FA were calculated and used for automatic clustering. Specifically, we calculated the correlations between blood traits and the ROI-based GM/FA across all subjects (corrected for age and TIV). Information about the correlation was stored in an *M*-by-*N* matrix, where *M* denotes the number of blood parameters and *N* denotes the number of ROIs. The correlation matrix was then *r*-to-*z* transformed (Fisher transformation). Then, the similarity in the correlation profiles between each pair of blood traits was quantified using the  $\eta^2$  coefficient (Cohen et al. 2008), resulting in an *M*-by-*M* symmetric matrix. A spectral clustering algorithm was used to automatically cluster (Ng et al. 2001) hematological and biochemical parameters separately. Spectral clustering is an unsupervised machine learning algorithm that groups variables that share similar correlations. The optimal number of clusters was evaluated by the Calinski–Harabasz (CH) index (Caliński and Harabasz 1974), which calculates the ratio of the between-cluster (*A*) to the within-cluster variance (*B*):  $CH = (A/B) \times (N - k)/(k - 1)$ , where *N* is the number of observations and *k* is the number of clusters. Generally, the optimal number was chosen as the one that maximizes the CH index, that is, when *A* is large and *B* is small. The higher the score the denser and better separated the clusters. The correlation profile of an individual blood parameter is defined as the spatial pattern of correlation coefficients between this parameter and the structural features of the GM/WM across the whole brain. The correlation profiles of parameters in the same cluster were averaged to obtain the correlation profile for each cluster.

Based on the results of the clustering, the reordered similarity matrices with respect to the cluster labels were converted to graphs for network analyses. Specifically, we converted each similarity matrix into a graph composed of modules that corresponded to clusters. Afterwards, we searched for the optimal threshold that maximized the graph modularity. Binary networks were then produced with the optimal threshold. We also calculated the ED and small-world property for each graph.

The network analyses in the present study were conducted using the Networkx package (v2.5, <https://networkx.org>), and graph plotting was conducted using Gephi (v0.9.2, <https://gephi.org>).

## Results

### Characteristics of the rhesus monkeys

The characteristics of the young adult, adult, and middle-aged adult macaques are presented in Table 1. There were significant differences between each pair of groups with respect to age and body weight. The young adults had significantly smaller TIVs than the middle-aged group. Both the young adults and adults had smaller WM volumes than the middle-aged group. There was no



**Table 1.** Demographic and neuroanatomical characteristics of macaques in this study<sup>a</sup>.

	All n = 36	Young adults n = 12	Adults n = 12	Middle-aged adults n = 12	Statistics <sup>b</sup>	
					F	p
Age, y	9.42 (4.02)	5.25 (0.75)	8.33 (0.49)	14.67 (0.49)	811.08	< 0.001
Age range, y	4–15	4–6	8–9	14–15		
Body weight, kg	7.62 (2.04)	5.30 (0.66)	8.03 (0.79)	9.53 (1.48)	64.25	< 0.001
TIV, cm <sup>3</sup>	108.71 (11.16)	102.82 (9.42)	107.86 (11.47)	115.45 (9.35)	5.33	.02
GM, cm <sup>3</sup>	47.25 (3.59)	46.28 (4.05)	47.39 (3.98)	48.08 (2.65)	0.81	n.s.
WM, cm <sup>3</sup>	37.30 (5.45)	33.49 (3.46)	36.33 (5.23)	42.08 (3.68)	17.04	< 0.001

GM, gray matter volume; TIV, total intracranial volume; WM, white matter volume. Mean and SD are reported unless otherwise specified. <sup>a</sup>All macaques were male. <sup>b</sup>Statistical analyses were performed between the young adults, adults, and middle-aged adults using analyses of variance. Post hoc tests revealed significant differences between each pair of groups for age and body weight; significantly smaller TIVs for the young adults than for the middle-aged adults; and significantly smaller WM for both the young adults and adults than for the middle-aged adults.

statistically significant difference in GM volume between the groups.

### Characteristics of biochemical and hematological parameters

The distributions and box plots of the biochemical and hematological parameters for blood measurements are reported in [Supplementary Figures S3–S6](#). We found that 16 out of 52 parameters showed significant differences between age groups (for details refer to [Supplementary Tables S2 and S3](#)). Bar plots of the first, second, and average of the 2 blood measurements are shown in [Supplementary Figures S7 and S8](#). Paired *t* tests between the two blood measurements showed that most of the parameters remained similar from the first sampling time to the second, but a few parameters fluctuated in the young (5 out of 52 parameters) or middle-aged group (4 out of 52 parameters, [Supplementary Table S4](#)). The reason that most of the blood parameters were stable may be because we used a relatively short interval between the first and second blood sampling, and each sampling was under relatively the same conditions and at the same time of day. The average of first and second measurements for 43 stable parameters were used in correlation analyses.

### Correlations between blood parameters and brain structures

To identify robust associations between blood parameters and brain tissues, we computed the average of 2 blood measurements for correlation analyses and inferences were made using a FDR approach with a threshold at  $P < 0.05$ . Correlations of the significant biochemical parameters against age are shown in [Supplementary Figure S9](#). We found that ALP ( $r = -0.60$ ) and HCY ( $r = 0.61$ ) changed with age, but we did not find significant correlations between other blood parameters and age or TIV. For the hematological parameters, significant positive associations were found between BASO and GM volumes in the anterior cingulum, the inferior, middle, and superior frontal gyri, and the superior temporal gyrus. HGB had negative correlations with putamen volume ([Fig. 1A](#)).

Detailed correlation results are shown in [Supplementary Table S5](#). Although correlations between biochemical parameters and GM volumes or WM integrity did not survive after multiple comparison corrections, we observed a trend that GGT and TC showed inverse correlations with the entorhinal and inferior temporal GM volumes, respectively, and GLU positively correlated with FA in the forceps major ([Supplementary Fig. S9](#)).

To gain panoramic information about the relationship between blood indices and the brain, covariation networks describing connections within the (1) blood parameters and (2) different brain structures as well as interactions between these 2 domains were reconstructed. The entire network consists of two modules. The blood module was constructed by pairwise correlations between each pair of hematological parameters. The brain structural module was constructed by pairwise correlations between each pair of gray or white matter ROIs (adjusted for age and TIV). Each module was binarized by  $P < 0.01$ . Correlations between the hematological measures and brain structures that had been FDR corrected  $P < 0.05$  were deemed to be connections between these 2 modules. Nodes with degree centrality in the top one third of all nodes were identified as the high degree hubs for each module. We observed that the high-degree hubs of the hematological and brain structural modules have connections with each other, suggesting that blood parameters have complex interactions with brain structures ([Fig. 1B](#)). The networks of hematological parameters and GM demonstrated small-world properties ( $\sigma = 1.80$ ). We observed higher interconnectivity within individual modules (ED = 0.1 and 0.18 for the hematological and GM modules, respectively) than that between the different modules (ED = 0.026, [Supplementary Table S6](#)).

### Clustering of biochemical and hematological parameters

Clustering was performed to automatically categorize blood indices such that indices with similar correlation profiles with whole brain were assigned to a common cluster, and indices with dissimilar correlation profiles with the whole brain were assigned to different clusters. As shown in [Supplementary Figure S10](#), a cluster number

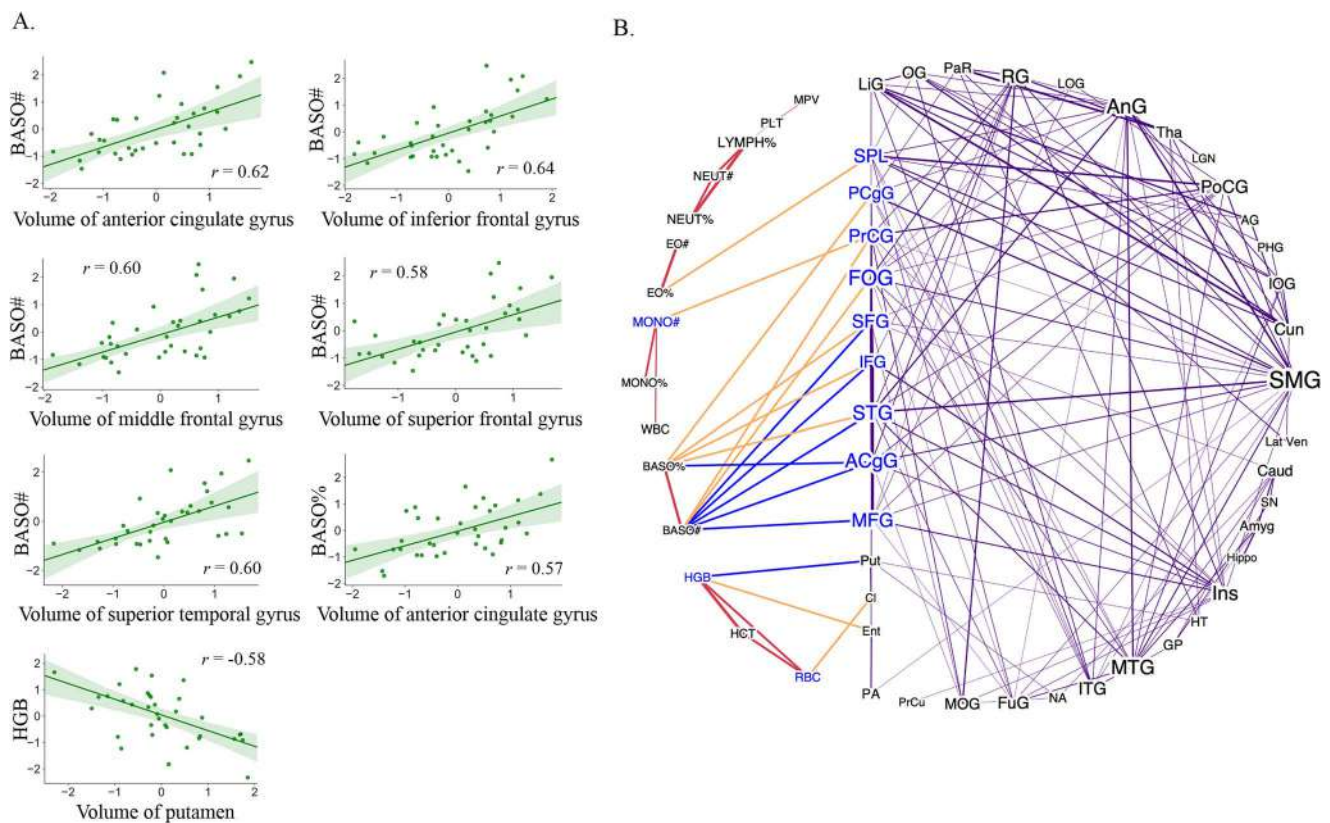


**Fig. 1.** Correlations between blood parameters and brain structures. (A) Scatter plots and the best linear fit displaying the correlations between hematological parameters and gray matter volumes of different areas. Shaded area represents the 95% confidence interval. False discovery rate corrected  $p < 0.05$ . BASO#, basophil count; BASO%, basophilic leukocyte percentage; HGB, hemoglobin. (B) Covariation networks showing the interactions between hematological parameters and gray matter volumes. Red lines indicate pairwise hematological correlations with  $P < 0.01$ . Purple lines indicate pairwise brain structural correlations with  $P < 0.01$ . Orange lines are correlations between hematological and structural correlations with  $P < 0.05$ . Blue lines show hematological and structural correlations with FDR corrected  $P < 0.05$ . These correlations are scatter plotted in A. The size of the nodes is proportioned according to the degree in each module. The width of the lines is proportioned according to the absolute correlation  $r$ . The blue nodes are high-degree network hubs with interdomain connections.

of 2 was optimal for clustering both the biochemical and hematological parameters.

The biochemical analyses revealed that liver enzyme activities (ALB, ALT, ALP, GGT, GLB, and TP), kidney function (CREA and UA), glucose, and lipid fractions (TG and HDL-C) were grouped together (Cluster 1) and were found to be positively correlated to the GM in the frontal cortex, insula, and superior temporal gyrus and were negatively correlated with GM in the inferior temporal gyrus, cuneus, and visual regions. Lipid fractions (TC and LDL-C) and liver enzymes activities (AST, DBIL, IDBIL, and TBIL) were in another cluster (Cluster 2) that was negatively associated with the frontal regions, inferior temporal gyrus, and amygdala volumes (Fig. 2A–D). The network similarity matrix derived from the biochemical measures and GM had a small-world property ( $\sigma = 2.33$ ), suggesting highly effective interactions among seemingly different modules of blood traits. We observed that the ED was smaller between the clusters (ED = 0.07) than within each of 2 clusters (ED = 0.37 for Cluster 1 and 0.30 for Cluster 2). Thus, the networks have dense connections between the nodes within each modules but sparse connections between nodes belonging to different modules. Biochemical clustering based on correlations with FA

revealed that lipid fractions (TC, TG, LDL-C, and HDL-C), kidney function (BUN, CREA, and UA), and glucose were classified into Cluster 1, which was positively correlated with the dorsal posterior corona radiata, forceps major, and cerebellum and that liver function indices (ALT, ALB, A/G, ALP, AST, DBIL, GGT, IDBIL, and TBIL) were categorized into Cluster 2 and were associated adversely with superior fronto-occipital fasciculus white matter integrity (Fig. 2E–H). Similarly, the network reconstructed by the similarity matrix also had small-world properties ( $\sigma = 1.30$ ), with EDs much smaller between the clusters (0.13) than within each of 2 clusters (0.6 for Cluster 1 and 0.32 for Cluster 2).

The same analyses were applied to the hematologic parameters. The hematologic clustering analysis revealed that erythrocyte and platelets had homogeneous association profiles with GM or FA and that these indices were negatively correlated with the frontal, inferior temporal, entorhinal, lingual, and visual GM volumes. The cluster that included erythrocytes and platelets showed inverse correlations with FA in the superior fronto-occipital fasciculus and positive correlations with FA in the anterior corona radiata. We observed that the leukocytes showed extensive positive correlations



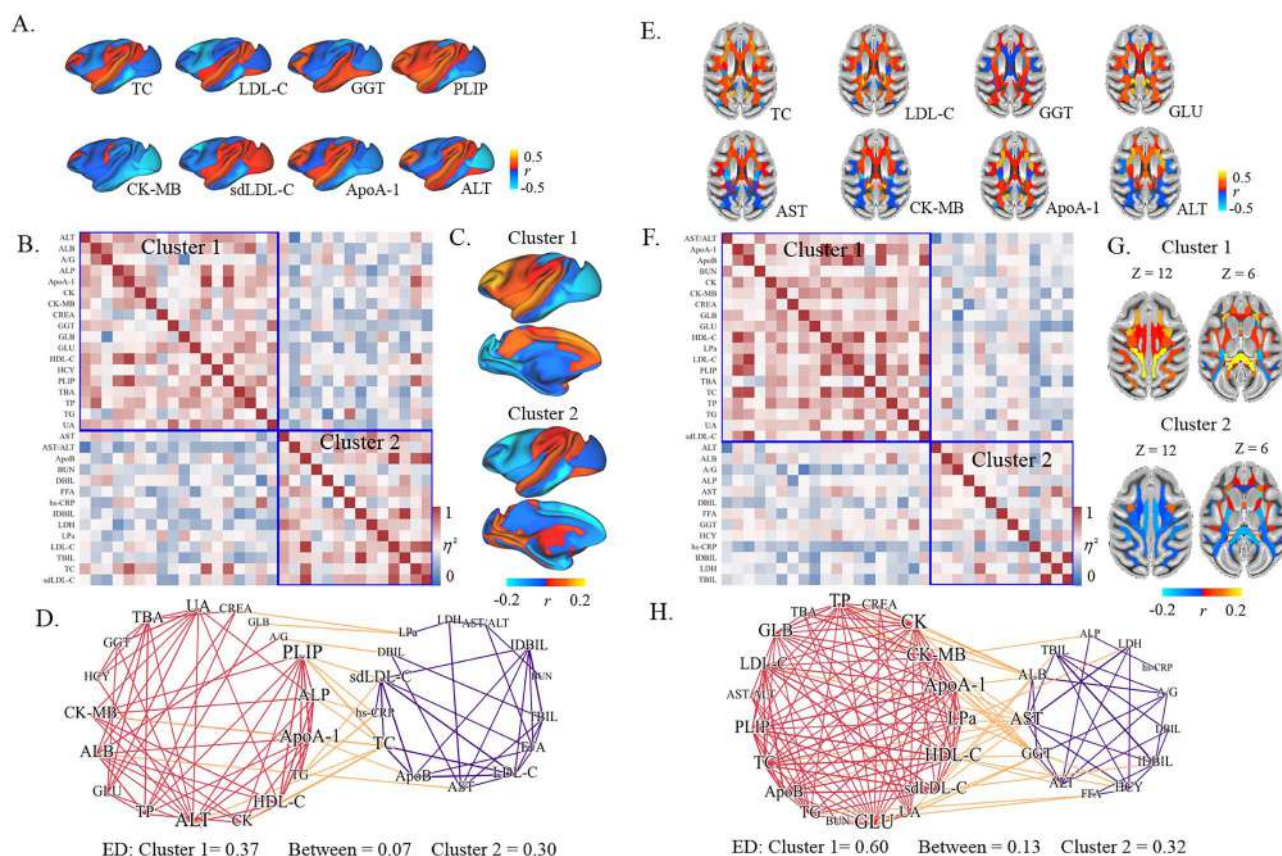


**Fig. 2.** Clustering of biochemical parameters based on their covariation with gray matter (A–D) and white matter structures (E–H) across the brain. A, Correlation profiles of randomly chosen 8 biochemical parameters with gray matter volume. B, The re-ordered similarity matrix with respect to the cluster labels. C, Average correlation profile with gray matter volume of each cluster. D, Network visualizing the correlations of the biochemical parameters. E, Correlation profiles of randomly chosen 8 biochemical parameter with the white matter integrity. F, The re-ordered similarity matrix with respect to the cluster labels. G, Average correlation profile with white matter integrity of each cluster. H, Network visualizing the correlations of biochemical parameters. Cluster 1 is shown as the red module and cluster 2 is shown as the purple module. Yellow lines show the connections between the 2 modules. The size of each node is proportional to the number of its connections (i.e., degree). The edge density within each cluster and between clusters is shown at the bottom of the graph.

with GM across widespread brain regions, including the frontal, temporal, insula, and precuneus regions and positive associations with FA in the forceps, superior fronto-occipital fasciculus, cingulum, and cerebellar peduncles (Fig. 3). Similar to the results obtained for the biochemical parameters, the networks of the similarity matrix derived from the hematological measures and GM/FA demonstrated the small-world property ( $\sigma = 1.41$  and 1.47, respectively), with higher interconnectivity with individual modules (ED = 0.42 and 0.3 for Cluster 1; ED = 0.6 and 0.75 for Cluster 2) than that between different modules (ED = 0.11 and 0.19).

## Discussion

This study investigated the associations between hematological/biochemical parameters and the brain's gray matter volume and white matter integrity derived from T1-weighted and diffusion MRI in rhesus monkeys. We found that intersubject variations in BASO and HGB levels were correlated with brain morphology. Specifically, BASO count was positively associated with GM volumes in the anterior cingulate, lateral frontal, and superior

temporal regions and that levels of HGB were inversely correlated with volumes in the putamen. Blood parameters tended to cluster into discrete groups in their correlations with various structures across the brain. Specifically, through intricate interactions between a number of key elements, the covariation network of both the hematological/biochemical parameters and the brain structures were linked to form a network with a hierarchical small-world property, suggesting that sophisticated yet highly effective interactions may exist between these domains. Furthermore, we found a variety of sub-networks of brain areas or fiber tracts that tended to interact with unique groups of blood indices, suggesting previously unknown interactions between physiological parameters of the body and the structural organization of the brain. Because many blood variables are risk factors for cerebrovascular and neurodegenerative diseases (Gokce et al. 2019; Harshfield et al. 2020), this study may have important implications for understanding the mechanisms connecting the physiological parameters of the body and the structural organization of the brain.

The reference ranges of most of the hematologic and serum biochemical values that we established were

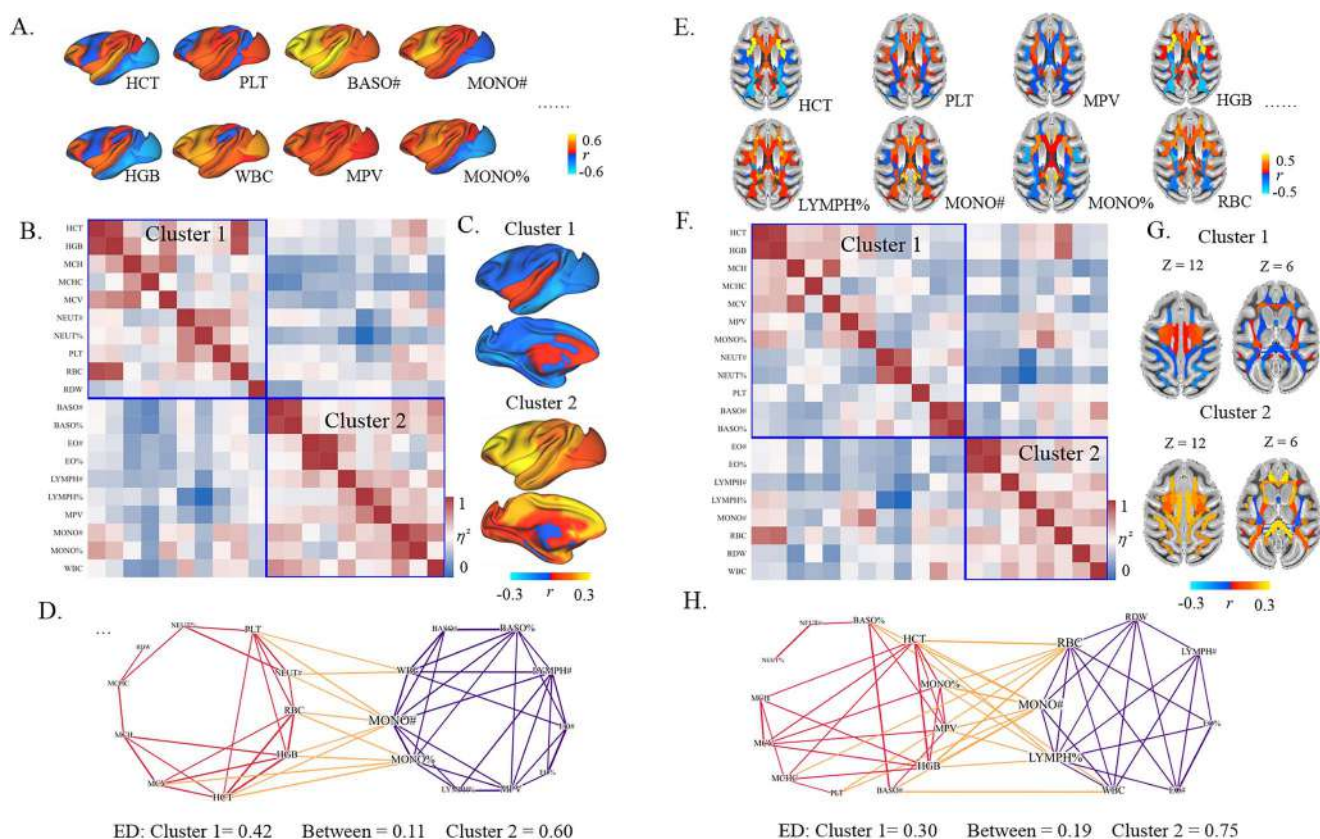


**Fig. 3.** Clustering of hematological parameters based on their covariation with gray matter (A-D) and white matter structures (E-H) across the brain. A, Correlation profiles of randomly chosen 8 hematological parameters with gray matter volume. B, The re-ordered similarity matrix with respect to the cluster labels. C, Average correlation profile with gray matter volume of each cluster. D, Network visualizing the correlations of the hematological parameters. E, Correlation profiles of randomly chosen 8 hematological parameter with the white matter integrity. F, The re-ordered similarity matrix with respect to the cluster labels. G, Average correlation profile with white matter integrity of each cluster. H, Network visualizing the correlations of hematological parameters. Cluster 1 is shown as the red module and cluster 2 is shown as the purple module. Yellow lines show the connections between the 2 modules. The size of each node is proportional to the number of its connections (i.e., degree). The edge density within each cluster and between clusters is shown at the bottom of the graph.

quantitatively similar to previous reports for macaques (Yu et al. 2019); the exceptions were LYMPH#, NEUT#, WBC, and UA. The discrepancies may be partially because of the geographic and environmental heterogeneity of the monkeys included in the 2 studies. Some physiologic variables changed with age in the NHPs. We observed apparent age-related changes in ALP and HCY. ALP is a marker for osteoblastic activity. The higher levels of ALP in young macaques are likely due to active bone formation. A similar effect of age on ALP levels has been found in cynomolgus (Xie et al. 2013), Tibetan (Wu et al. 2014), and vervet (Sato et al. 2005) monkeys. We observed that HCY levels increased with age, a finding which has also been reported in studies involving humans (Marlatt et al. 2008).

The present study identified associations between blood traits and brain structures and analyzed them from a network perspective. Specifically, the BASO count was positively associated with GM volumes in the anterior cingulate, lateral prefrontal, and superior temporal regions, and the levels of HGB were inversely correlated with volumes in the putamen. Basophils play a role in allergic inflammations and release histamine in allergic

reactions. The histamine system is involved in various biological functions, such as emotion, memory, anxiety, and reward (Dere et al. 2010). The link between BASO and the brain has scarcely been investigated. Previous studies reported that elevated BASO was associated with increased fluid intelligence scores (Klinedinst et al. 2019) and that reduced BASO had a negative effect that is associated with mood disorders (Baek et al. 2016). However, the underlying mechanisms between BASO and behaviors or brain health are not well elucidated. The anterior cingulate cortex lies in the medial wall of the cortex with extensive connections with the limbic system and prefrontal cortex, which are known to be important for emotion, memory, and cognitive processing (Bush et al. 2000; Stevens et al. 2011). The prefrontal cortex is a critical region for emotion, cognition, and emotion-cognition integration (Gray et al. 2002). The present study identified a link between BASO and the anterior cingulate, prefrontal, and temporal GM volumes, suggesting that these regions may act as physiologic substrates for the associations between BASO and brain health/behaviors. HGB is the iron-containing oxygen-transport metalloprotein in erythrocytes. Human studies



have demonstrated that low levels of HGB (anemia) are associated with adverse health conditions (Wolters et al. 2019). In addition, studies of the full range of HGB found that high levels of HGB were also associated with increased risk of dementia (Shah et al. 2011; Wolters et al. 2019) and cardiovascular disease (Gotoh et al. 2015; Wolters et al. 2019), suggesting that high levels of HGB may be deleterious (Wolters et al. 2019). The present study found that the HGB levels were inversely correlated with the volumes of the putamen. The putamen is part of the basal ganglia nucleus and supports a variety of motor and cognitive functions. Previous studies showed that the putamen is involved in the degeneration of neurons in neurodegenerative diseases, including dementia (de Jong et al. 2008) and Parkinson's disease (Playford et al. 1992). Our finding suggested that the putamen may be a potential key area for understanding the associations between high levels of HGB and brain health.

In addition to the above-mentioned specific correlations, another contribution of the present work is that it used network analysis to provide a panoramic picture of the relationship between multiple blood parameters and brain structural features. We found that HGB was identified as a high-degree hematological network hub and was closely connected with the brain structural network; from the brain perspective, the cingulum and prefrontal cortex were high-degree hubs in the brain structural network and were connected with the hematological domain. As a result, the system exhibits a strong small-world property, suggesting that interactions can propagate through the entire network in a highly effective manner, thereby connecting the seemingly different domains of blood traits and brain structures.

The investigation into covariation in brain structures based on their associations with blood traits revealed various patterns of brain organization in macaques, suggesting that brain structures may have complex interactions with the variations in blood traits in normal subjects. This is the first systematic study of the relationship between hematologic and chemistry parameters and brain macro- and micro-structures in macaques from a network perspective. We identified clusters of blood parameters that interact with largely different sets of brain regions. Specifically, for the biochemical parameters, Cluster 1 consisted of liver enzyme activities (ALB, ALT, ALP, GGT, GLB, and TP), kidney function (CREA and UA), glucose, and lipid fractions (TG and HDL-C), and these parameters positively correlated with GM volumes in the prefrontal cortex, insula, and superior temporal gyrus, and negatively correlated with GM in the inferior temporal gyrus, cuneus, and visual cortex. Cluster 2 included lipid fractions (TC and LDL-C) and liver enzymes activities (AST, DBIL, IDBIL, and TBIL), which were inversely associated with the prefrontal cortex, inferior temporal gyrus, and amygdala volumes. These results reveal a previously unknown brain structural organization in which specific groups of brain areas are

possibly affected by different physiological processes. We acknowledge that the causal relationships between these blood indices and the brain are still unclear, and future work with animal models may provide the capacity to demonstrate causal links between these two domains.

The network analyses demonstrated that the blood networks had small-world properties. Small-world networks are formed by strong clustering with similar correlation profiles within modules and by a small number of interactions that bridge the groups of distinct correlation patterns. Small-world architectures have been found in many complex systems, including brain networks (Yu et al. 2008; Bullmore and Sporns 2009), and have been widely considered as an essential design for increasing the efficiency of network interactions at both the local and global scales. Here we demonstrated that the overarching network connecting the blood traits and the brain exhibited a hierarchical small-world architecture and was manifested between (1) 2 domains of the blood indices and the brain structural features, and (2) the 2 subdomains of the blood indices. This implies that there are sophisticated links between blood traits and brain structural features. With a high global and local efficiency of interactions, the networks we revealed here allow changes in the status of individual nodes (e.g. blood traits or brain structural features) to propagate through the whole network, potentially leading to a system-wide adaptive reconfiguration.

A limitation of the present study is that the number of macaques included in the analysis was relatively small compared with human studies. Future work with a larger sample size would be helpful for further investigating the relationship between blood traits and brain structure.

In conclusion, the present study provides *in vivo* evidence that biochemical and hematological parameters link brain macro- and micro-structures in macaques. Novel and diverse brain structural organizations were revealed by blood traits that correlated with brain structures. This comprehensive analysis of the relationship between blood indices and tissues throughout the whole brain suggests complex interactions between these two domains. The present study established comprehensive baseline reference indices for rhesus monkeys that correlate with brain structural features, suggesting that the surveillance or control of blood indicators may be indispensable when constructing and evaluating various central nervous system disease models using NHPs. In addition, the relationships between blood traits and brain structural features in NHPs revealed here can contribute to a better understanding of the interaction between physiologic variables of the body and the brain across species.

## Acknowledgement

The authors thank Drs Rhoda E. and Edmund F. Perozzi for English editing on the manuscript.

## Supplementary material

Supplementary material is available at *Cerebral Cortex Journal* online.

## Funding

This work was supported by the National Key Research and Development Program of China (2017YFA0105203 and 2017YFA0105201), the National Science Foundation of China (31771076 and 81925011), the Strategic Priority Research Program of the Chinese Academy of Sciences (CAS) (XDB32040201), Key-Area Research and Development Program of Guangdong Province (2019B030335001), and the Beijing Advanced Discipline Fund.

*Conflict of interest statement.* The authors declare that they have no competing financial interests.

## Data availability

The data that support the findings of this study can be obtained from the corresponding authors upon reasonable request.

## References

- Alexander GE, Chen K, Aschenbrenner M, Merkley TL, Santerre-Lemmon LE, Shamy JL, Skaggs WE, Buonocore MH, Rapp PR, Barnes CA. Age-related regional network of magnetic resonance imaging gray matter in the rhesus macaque. *J Neurosci*. 2008;28:2710–2718.
- Baek JH, Kim H-J, Fava M, Mischoulon D, Papakostas GI, Nierenberg A, Heo J-Y, Jeon HJ. Reduced venous blood basophil count and anxious depression in patients with major depressive disorder. *Psychiatry Investig*. 2016;13(3):321–326.
- Bullmore E, Sporns O. Complex brain networks: graph theoretical analysis of structural and functional systems. *Nat Rev Neurosci*. 2009;10:186–198.
- Burtis CA, Ashwood ER, Bruns DE. *Tietz textbook of clinical chemistry and molecular diagnostics-e-book*. Elsevier Health Sciences; 2012
- Bush G, Luu P, Posner MI. Cognitive and emotional influences in anterior cingulate cortex. *Trends Cogn Sci*. 2000;4:215–222.
- Caliński T, Harabasz J. A dendrite method for cluster analysis. *Commun Stat Theory Methods*. 1974;3:1–27.
- Chen X, Errangi B, Li L, Glasser MF, Westlye LT, Fjell AM, Walhovd KB, Hu X, Herndon JG, Preuss TM, et al. Brain aging in humans, chimpanzees (*Pan troglodytes*), and rhesus macaques (*Macaca mulatta*): magnetic resonance imaging studies of macro- and micro-structural changes. *Neurobiol Aging*. 2013;34:2248–2260.
- Cohen AL, Fair DA, Dosenbach NU, Miezin FM, Dierker D, van Essen DC, Schlaggar BL, Petersen SE. Defining functional areas in individual human brains using resting functional connectivity MRI. *NeuroImage*. 2008;41:45–57.
- Coutinho AM, Coutu J-P, Lindemer ER, Rosas HD, Rosen BR, Salat DH. Differential associations between systemic markers of disease and cortical thickness in healthy middle-aged and older adults. *NeuroImage*. 2017;146:19–27.
- Curran EK, Godfrey J, Kline J. Mechanisms of immune tolerance in leukemia and lymphoma. *Trends Immunol*. 2017;38:513–525.
- de Jong LW, van der Hiele K, Veer IM, Houwing J, Westendorp R, Bollen E, de Bruin PW, Middelkoop H, van Buchem MA, van der Grond J. Strongly reduced volumes of putamen and thalamus in Alzheimer's disease: an MRI study. *Brain*. 2008;131:3277–3285.
- Dere E, Zlomuzica A, de Souza Silva MA, Ruocco L, Sadile A, Huston J. Neuronal histamine and the interplay of memory, reinforcement and emotions. *Behav Brain Res*. 2010;215:209–220.
- Feng L, Jeon T, Yu Q, Ouyang M, Peng Q, Mishra V, Pletikos M, Sestan N, Miller MI, Mori S, et al. Population-averaged macaque brain atlas with high-resolution ex vivo DTI integrated into in vivo space. *Brain Struct Funct*. 2017;222:4131–4147.
- Gibbs RA, Rogers J, Katze MG, Bumgarner R, Weinstock GM, Mardis ER, Remington KA, Strausberg RL, Venter JC, Wilson RK. Evolutionary and biomedical insights from the rhesus macaque genome. *Science*. 2007;316:222–234.
- Gokce M, Bektay MY, Selvitop R, Toprak A, Yildiz GB. Investigation of the effects of biochemical parameters on Alzheimer's disease. *Am J Alzheimers Dis Other Dement*. 2019;34:464–468.
- Gotoh S, Hata J, Ninomiya T, Hirakawa Y, Nagata M, Mukai N, Fukuhara M, Ikeda F, Ago T, Kitazono T, et al. Hematocrit and the risk of cardiovascular disease in a Japanese community: the Hisayama study. *Atherosclerosis*. 2015;242:199–204.
- Gray DT, Barnes CA. Experiments in macaque monkeys provide critical insights into age-associated changes in cognitive and sensory function. *Proc Natl Acad Sci U S A*. 2019;116:26247–26254.
- Gray JR, Braver TS, Raichle ME. Integration of emotion and cognition in the lateral prefrontal cortex. *Proc Natl Acad Sci U S A*. 2002;99:4115–4120.
- Harshfield EL, Sims MC, Traylor M, Ouwehand WH, Markus HS. The role of haematological traits in risk of ischaemic stroke and its subtypes. *Brain*. 2020;143:210–221.
- Jung B, Taylor PA, Seidlitz J, Sponheim C, Perkins P, Ungerleider LG, Glen D, Messinger A. A comprehensive macaque fMRI pipeline and hierarchical atlas. *NeuroImage*. 2021;235:117997.
- Kalay N, Dogdu O, Koc F, Yarlioglu M, Ardic I, Akpek M, Cicek D, Oguzhan A, Ergin A, Kaya MG. Hematologic parameters and angiographic progression of coronary atherosclerosis. *Angiology*. 2012;63:213–217.
- Kim J, Jung Y, Barcus R, Bachevalier JH, Sanchez MM, Nader MA, Whitlow CT. Rhesus macaque brain developmental trajectory: a longitudinal analysis using tensor-based structural morphometry and diffusion tensor imaging. *Cereb Cortex*. 2020;30:4325–4335.
- Klinedinst BS, Pappas C, Le S, Yu S, Wang Q, Wang L, Allenspach-Jorn K, Mochel JP, Willette AA. Aging-related changes in fluid intelligence, muscle and adipose mass, and sex-specific immunologic mediation: a longitudinal UK biobank study. *Brain Behav Immun*. 2019;82:396–405.
- Leritz EC, Salat DH, Williams VJ, Schnyer DM, Rudolph JL, Lipsitz L, Fischl B, McGlinchey RE, Milberg WP. Thickness of the human cerebral cortex is associated with metrics of cerebrovascular health in a normative sample of community dwelling older adults. *NeuroImage*. 2011;54:2659–2671.
- Makris N, Papadimitriou GM, van der Kouwe A, Kennedy DN, Hodge SM, Dale AM, Benner T, Wald LL, Wu O, Tuch DS, et al. Frontal connections and cognitive changes in normal aging rhesus monkeys: a DTI study. *Neurobiol Aging*. 2007;28:1556–1567.
- Mapstone M, Cheema AK, Fiandaca MS, Zhong X, Mhyre TR, MacArthur LH, Hall WJ, Fisher SG, Peterson DR, Haley JM, et al. Plasma phospholipids identify antecedent memory impairment in older adults. *Nat Med*. 2014;20:415–418.
- Marlatt MW, Lucassen PJ, Perry G, Smith MA, Zhu X. Alzheimer's disease: cerebrovascular dysfunction, oxidative stress, and advanced clinical therapies. *J Alzheimers Dis*. 2008;15:199–210.
- Nägga K, Gustavsson A-M, Stomrud E, Lindqvist D, van Westen D, Blennow K, Zetterberg H, Melander O, Hansson O. Increased

- midlife triglycerides predict brain  $\beta$ -amyloid and tau pathology 20 years later. *Neurology*. 2018;90:e73–e81.
- Nambron R, Silajdžić E, Kalliolia E, Ottolenghi C, Hindmarsh P, Hill NR, Costelloe SJ, Martin NG, Positano V, Watt HC, et al. A metabolic study of Huntington's disease. *PLoS One*. 2016;11:e0146480.
- Ng AY, Jordan MI, Weiss Y. 2001. On spectral clustering: analysis and an algorithm. *Proceedings of Advances in Neural Information Processing Systems* Cambridge, MA: MIT Press. 14:849–856.
- Playford E, Jenkins I, Passingham R, Nutt J, Frackowiak R, Brooks D. Impaired mesial frontal and putamen activation in Parkinson's disease: a positron emission tomography study. *Ann Neurol*. 1992;32:151–161.
- Power MC, Tingle JV, Reid RI, Huang J, Sharrett AR, Coresh J, Griswold M, Kantarci K, Jack CR Jr, Knopman D, et al. Midlife and late-life vascular risk factors and white matter microstructural integrity: the atherosclerosis risk in communities neurocognitive study. *J Am Heart Assoc*. 2017;6:e005608.
- Qiu C, Zhang Y, Bronge L, Herlitz A, Aspelin P, Bäckman L, Fratiglioni L, Wahlund LO. Medial temporal lobe is vulnerable to vascular risk factors in men: a population-based study. *Eur J Neurol*. 2012;19:876–883.
- Rilling JK. Comparative primate neuroimaging: insights into human brain evolution. *Trends Cogn Sci*. 2014;18:46–55.
- Rohlfing T, Koenke CD, Sullivan EV, Dubach MF, Bowden DM, Grant K, Pfefferbaum A. The INIA19 template and NeuroMaps atlas for primate brain image parcellation and spatial normalization. *Front Neuroinform*. 2012;6:27.
- Sampaio-Baptista C, Khrapitchev AA, Foxley S, Schlagheck T, Scholz J, Jbabdi S, DeLuca GC, Miller KL, Taylor A, Thomas N, et al. Motor skill learning induces changes in white matter microstructure and myelination. *J Neurosci*. 2013;33:19499–19503.
- Sato A, Fairbanks LA, Lawson TP, Lawson GW. Effects of age and sex on hematologic and serum biochemical values of vervet monkeys (*Chlorocebus aethiops sabaeus*). *J Am Assoc Lab Anim Sci*. 2005;44:29–34.
- Schilling S, Tzourio C, Dufouil C, Zhu Y, Berr C, Alperovitch A, Crivello F, Mazoyer B, Dobbie S. Plasma lipids and cerebral small vessel disease. *Neurology*. 2014;83:1844–1852.
- Scott JA, Grayson D, Fletcher E, Lee A, Bauman MD, Schumann CM, Buonocore MH, Amaral DG. Longitudinal analysis of the developing rhesus monkey brain using magnetic resonance imaging: birth to adulthood. *Brain Struct Funct*. 2016;221:2847–2871.
- Shah R, Buchman A, Wilson R, Leurgans S, Bennett D. Hemoglobin level in older persons and incident Alzheimer disease: prospective cohort analysis. *Neurology*. 2011;77:219–226.
- Stevens FL, Hurley RA, Taber KH. Anterior cingulate cortex: unique role in cognition and emotion. *J Neuropsychiatry Clin Neurosci*. 2011;23:121–125.
- Tournier JD, Calamante F, Connelly A. MRtrix: diffusion tractography in crossing fiber regions. *Int J Imaging Syst Technol*. 2012;22:53–66.
- Tuch DS, Salat DH, Wisco JJ, Zaleta AK, Hevelone ND, Rosas HD. Choice reaction time performance correlates with diffusion anisotropy in white matter pathways supporting visuospatial attention. *Proc Natl Acad Sci U S A*. 2005;102:12212–12217.
- Van Essen DC, Donahue CJ, Coalson TS, Kennedy H, Hayashi T, Glasser MF. Cerebral cortical folding, parcellation, and connectivity in humans, nonhuman primates, and mice. *Proc Natl Acad Sci U S A*. 2019;116:26173–26180.
- Vanduffel W, Zhu Q, Orban GA. Monkey cortex through fMRI glasses. *Neuron*. 2014;83:533–550.
- Whalley L, Staff R, Murray A, Duthie S, Collins A, Lemmon H, Starr J, Deary I. Plasma vitamin C, cholesterol and homocysteine are associated with grey matter volume determined by MRI in nondemented old people. *Neurosci Lett*. 2003;341:173–176.
- Willette AA, Gallagher C, Bendlin BB, McLaren DG, Kastman EK, Canu E, Kosmatka KJ, Field AS, Alexander AL, Colman RJ, et al. Homocysteine, neural atrophy, and the effect of caloric restriction in rhesus monkeys. *Neurobiol Aging*. 2012;33:670–680.
- Williams VJ, Leritz EC, Shepel J, McGlinchey RE, Milberg WP, Rudolph JL, Lipsitz LA, Salat DH. Interindividual variation in serum cholesterol is associated with regional white matter tissue integrity in older adults. *Hum Brain Mapp*. 2013;34:1826–1841.
- Wolters FJ, Zonneveld HI, Licher S, Cremers LG, on behalf of the Heart Brain Connection Collaborative Research Group, on behalf of the Heart Brain Connection Collaborative Research Group, Ikram MK, Koudstaal PJ, Vernooij MW, Ikram MA, et al. Hemoglobin and anemia in relation to dementia risk and accompanying changes on brain MRI. *Neurology*. 2019;93:e917–e926.
- Wu D, Yi Y, Sun F, Zhou L, Yang F, Wang H, Zhang G, Zhang YA, Yue F. Effects of age and sex on the hematology and blood chemistry of Tibetan macaques (*Macaca thibetana*). *J Am Assoc Lab Anim Sci*. 2014;53:12–17.
- Xie L, Xu F, Liu S, Ji Y, Zhou Q, Wu Q, Gong W, Cheng K, Li J, Li L, et al. Age- and sex-based hematological and biochemical parameters for *Macaca fascicularis*. *PLoS One*. 2013;8:e64892.
- Xu T, Falchier A, Sullivan EL, Linn G, Ramirez JS, Ross D, Feczko E, Opitz A, Bagley J, Sturgeon D, et al. Delineating the macroscale areal organization of the macaque cortex in vivo. *Cell Rep*. 2018;23:429–441.
- Xu T, Nanning K-H, Schwartz E, Hong S-J, Vogelstein JT, Goulas A, Fair DA, Schroeder CE, Margulies DS, Smallwood J, et al. Cross-species functional alignment reveals evolutionary hierarchy within the connectome. *NeuroImage*. 2020;223:117346.
- Yang FN, Stanford M, Jiang X. Low cholesterol level linked to reduced semantic fluency performance and reduced gray matter volume in the medial temporal lobe. *Front Aging Neurosci*. 2020;12:57.
- Yu S, Huang D, Singer W, Nikolić D. A small world of neuronal synchrony. *Cereb Cortex*. 2008;18:2891–2901.
- Yu W, Hao X, Yang F, Ma J, Zhao Y, Li Y, Wang J, Xu H, Chen L, Liu Q, et al. Hematological and biochemical parameters for Chinese rhesus macaque. *PLoS One*. 2019;14:e0222338.